© 2017. Published by The Company of Biologists Ltd | Journal of Experimental Biology (2017) 220, 3142-3153 doi:10.1242/jeb.159244

RESEARCH ARTICLE

# Estimation of distance and electric impedance of capacitive objects in the weakly electric fish *Gnathonemus petersii*

**Martin Gottwald*, Raya A. Bott and Gerhard von der Emde**


## ABSTRACT

During active electrolocation, the weakly electric fish *Gnathonemus petersii* judges the distance and impedance of nearby objects. Capacitive objects, which modulate local amplitude and waveform of the fish's electric probing signals, cast amplitude and waveform images onto the fish's electroreceptive skin. For an unambiguous estimation of the impedance and distance of an object, the animal has to deal with multiple dependencies of object and image parameters. Based on experimentally recorded amplitude and waveform images, we investigated possible strategies of the fish to unequivocally determine both the distance and the impedance of capacitive objects. We show that the relative slope in amplitude images, but not in waveform images, is independent of object impedance and is a measure of object distance. Distance-invariant impedance estimators were obtained by two different analytical strategies. The peak modulations of both image types were 'calibrated' with the relative slope of the amplitude image. Impedance estimators were obtained whenever these pairs of image features (peak and relative slope) were related dynamically over two consecutive distances. A static impedance estimator termed 'electric colour' is postulated to arise from the relationship of an amplitude and waveform image. Our results confirm that electric colour is indeed unaffected by object distance. For electric colour estimation we suggest a minimalistic approach of just relating the peak modulations of both image types to the basal amplitude and waveform condition. Our results are discussed with regard to the anatomical and physiological organization of the fish's electrosensory neuronal pathways and behavioural strategies of electrolocating fish.


**KEY WORDS: Active electrolocation, Electric image, Distance estimation, Impedance estimation, Electric colour**

## INTRODUCTION

In active sensory systems, recognition of specific object features often requires a compensation of multi-parametrical dependencies. The active electric sense of the weakly electric fish *Gnathonemus petersii* (Mormyridae) is an interesting model to study image processing and behavioural strategies for unambiguous feature extraction. Being nocturnal, the animal employs its active electric sense for short-range orientation and foraging (active electrolocation). During active electrolocation, the fish generates an electric field around its body by emitting biphasic current pulses (electric organ discharges, EODs) with an electric organ (EO) in the tail (Bell et al., 1976; Harder et al., 1964). Electroreceptor organs are spread across the fish's back and belly, and at a higher density at the head and chin appendix (Harder, 1968; von der Emde and Schwarz, 2002). They detect the electric pulses at the fish's skin, which are called local EODs (lEODs).

Two types of receptor cells – A cells and B cells – within each electroreceptor organ monitor the peak-to-peak (PP; Fig. 1) amplitude (A cells) or amplitude and waveform (B cells) of the lEODs (Szabo and Wersäll, 1970; von der Emde and Bleckmann, 1992). Both parameters are altered by nearby objects with electrical impedances different from that of water. Purely resistive objects (e.g. stones, dead wood, sand) modulate the lEOD amplitude only. Capacitive objects [e.g. other fish, plants and prey (insect larvae)] also modulate or 'distort' the lEOD waveform (von der Emde and Schwarz, 2002). A measure to quantify the lEOD waveform distortion is the so-called P/N ratio (von der Emde, 1990), which is the absolute ratio of the positive to negative lEOD peaks (Fig. 1). Object-induced lEOD modulations across the fish body form so-called electric images. By modulating the lEOD amplitudes and waveforms on the fish skin (Budelli and Caputi, 2000), capacitive objects generate an amplitude and a waveform image. Electric images encode the spatial dimensions, distance and electrical impedance of nearby objects.

Over the past years, modelling and measurement studies complemented by behavioural data (Budelli and Caputi, 2000; Caputi et al., 1998; Hofmann et al., 2012; von der Emde et al., 1998) have revealed many details of electric image profiles and uncovered crucial image features for object analysis. However, almost all of these studies focused solely on amplitude images of purely resistive objects.

Amplitude images have a reverse centre-surround (or 'Mexican hat') profile (Caputi et al., 1998). As these modulation profiles are sculpted by the impedance, size, shape and distance of an object, image features are influenced by many parameters (von der Emde and Schwarz, 2002). An unambiguous cue for distance estimation, however, is the relative slope of the amplitude image (Caputi et al., 1998; Hofmann et al., 2012; Sicardi et al., 2000; von der Emde et al., 1998). It is defined as the ratio of the steepest slope to the strongest modulation of the image (von der Emde et al., 1998). The relative slope is hypothesized to be the crucial factor to compensate for object distance during further feature extractions, e.g. impedance estimation (von der Emde and Schwarz, 2002). The mechanism underlying such a calibration process is as yet unknown.

Another parameter for distance-invariant impedance estimation in *G. petersii* was introduced in a modelling study by Budelli and Caputi (2000). It is calculated from the linear relationship of amplitude and waveform image modulations as a slope value. By analogy to colour perception in vision, which is also attained by relating the inputs of at least two different receptor types, it is referred to as the 'electric colour' of an object. So far, there is still a lack of electric image measurements or behavioural studies to complement this modelling effort.

Department of Neuroethology/Sensory Ecology, Institute of Zoology, Bonn University, 53115 Bonn, Germany.

*Author for correspondence (martingottwald@uni-bonn.de)

M.G., 0000-0001-8486-126X

**Received 9 March 2017; Accepted 23 June 2017**



Journal of Experimental Biology

Journal of Experimental Biology (2017) 220, 3142-3153 doi:10.1242/jeb.159244

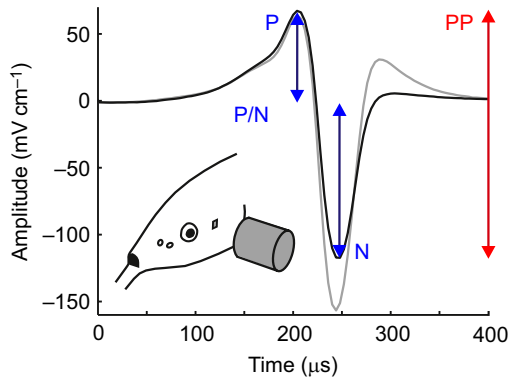


**Fig. 1. Local electric organ discharge (lEOD) and lEOD signal parameters.** Waveforms of two lEODs recorded close to the side of the head (grey rectangle to the right of the eye) of a discharging *Gnathonemus petersii*. Compared with a lEOD without an object (black line), a capacitive (4 nF) dipole object (grey cylinder) modulates the peak-to-peak (PP) amplitude (red double arrow) and the ratio of the peak amplitudes (blue double arrows) of the positive (P) and negative (N) phase, by distorting the lEOD waveform (grey line).

In this paper, we explored the electric image parameters and computational strategies underlying distance and impedance estimation of capacitive objects. We present high-resolution electric image recordings of artificial (dipole objects) and natural capacitive objects at different distances from the side of the fish's head. The profiles of amplitude and, for the first time, also of waveform images are analysed in detail. We hypothesize that the relative slopes of amplitude but also of waveform images mediate distance estimation. We further tested the hypothesis that a calibration routine based on relative image slopes provides distance-invariant impedance measures and propose a detailed mechanism. Finally, we evaluated the possibility of distance-independent impedance detection by using electric colour.

## MATERIALS AND METHODS

### Experimental animals

Electric image data were obtained from three *G. petersii* (Günther 1862) (length ∼15 cm) of unspecified sex and age. The animals were purchased from a local fish dealer (Aquarium Glaser, Rodgau Hessen, Germany). Fish were housed in separate tanks (60 l) at a water temperature of 26±1°C and an electrical conductivity of 100±10 μS cm$^{-1}$, with a 12 h:12 h light:dark cycle.

Experiments were carried out in accordance with the guidelines of German law and with the animal welfare regulations of the University of Bonn. All procedures and methods were approved by the LANUV NRW (Landesamt für Natur, Umwelt und Verbraucherschutz Nordrhein-Westfalen, reference number: 84-02.04.2015.A444).

### Recording of lEOD modulations: basic procedure

Prior to recordings, fish received initial anaesthesia by Ethomidate (2 mg ml$^{-1}$, Janssen-Cilag GmbH, Neuss North Rhine-Westfalia, Germany) using a concentration of 0.6 ml Ethomidate in 1 litre of water. While anaesthesia drastically reduced movement of the fish and slowed down EOD emission rate (∼1 Hz), EOD amplitude and waveform were unaffected (Engelmann et al., 2006), and fish could still ventilate autonomously.

Immobilized fish were then fixed onto a central Styrofoam holder (6×9×2 cm) in the experimental tank (38.5×28.7×18.8 cm) using four pairs of wooden sticks and cloth strings. To sustain anaesthesia during experiments, the tank water (26±1°C; 100±5 μS cm$^{-1}$) had a concentration of 0.3 ml Ethomidate per litre. Using a micromanipulator, artificial or natural capacitive objects were positioned close to the side of the fish head. lEOD recordings were performed with a self-made carbon dipole electrode (2 mm pole length, 1 mm inter-pole-distance), placed between the object and the fish skin, with the carbon poles orientated perpendicular to the rostro-caudal axis of the fish. Electrode positioning was achieved by a computer-guided motor-system, allowing precise movements in the $x$ (rostro-caudal), $y$ (dorso-ventral) and $z$ (lateral) directions. Local EODs were amplified (custom-built differential amplifier, ×100), filtered (band-pass: 1 Hz to 100 kHz) and digitized (A/D converter, sampling rate 250 kHz; PCIe 6341, National Instruments, Austin, TX, USA). A self-designed LabVIEW program (National Instruments) was used to monitor the recordings, to process lEOD modulations and to visualize and store the data. To define the object-evoked, mean lEOD amplitude (calculated as PP) and waveform (calculated as P/N) modulation close to a particular skin position, lEODs ($n$≥5) were recorded in the presence and absence of an object. PP and P/N modulation was then calculated by dividing the means of the PP or P/N values obtained with an object by those obtained without an object. In addition, the basal PP and P/N condition at a particular position, which is a baseline occurring without any object, was calculated by dividing the means of PP or P/N values measured in two successive trials in the absence of any object.

During the experiments, two different recording routines were applied for (i) preliminary recordings of dipole objects (see 'Artificial capacitive objects', below) and (ii) spatial electric image recordings of dipole objects and natural capacitive objects (see 'Recording of electric images', below).

### Artificial capacitive objects

A cylindrical dipole object (8×8 mm; volume 0.4 cm$^3$) was used to create artificial capacitive objects during the experiments. The front and back of the cylinder were made of carbon and the curved surface was coated with electrical insulating varnish. Both carbon poles were internally wired and connected to a variable resistance/capacitance circuit. By changing circuit settings, resistive and capacitive dipole objects were generated, which induce a wide range of lEOD amplitude (PP) and waveform (measured as P/N) modulations, similar to those caused by natural objects (von der Emde, 1990). A quick experimental assessment of the range of dipole object-evoked PP and P/N modulations was achieved by performing lEOD recordings at only a single spot close to the fish skin (von der Emde and Ronacher, 1994). Thus, only a single central pixel within the electric images was analysed. Following this procedure, we quantified PP and P/N modulations of capacitive ($n$=11, 0.5–1000 nF) and resistive ($n$=9, 0 Ω to 1 MΩ) dipole objects to select circuit settings for further electric image measurements. Object-evoked modulations were obtained for 5 and 8 mm object distance and for selected circuit settings (4, 30 nF), over a larger range of object-to-fish distances (see Fig. 2A for details). In addition, the basal PP and P/N conditions were acquired. For recordings ($n$=20 lEODs per setting), the electrode was positioned between the eye and the gill opening at 2 mm distance to the side of the head of a discharging *G. petersii* (Fig. 2A). The dipole cylinder was orientated perpendicular to the electrode and the fish's skin (Fig. 2A).

Fig. 2A shows the PP–P/N modulation pairs, recorded for a given object, in a 2D space with the stimulus dimensions amplitude and waveform on its axis. PP modulations below 1 were obtained when the dipole object had a higher resistance than the surrounding water; PP modulations larger than 1 are caused by dipole objects with a

Journal of Experimental Biology (2017) 220, 3142-3153 doi:10.1242/jeb.159244

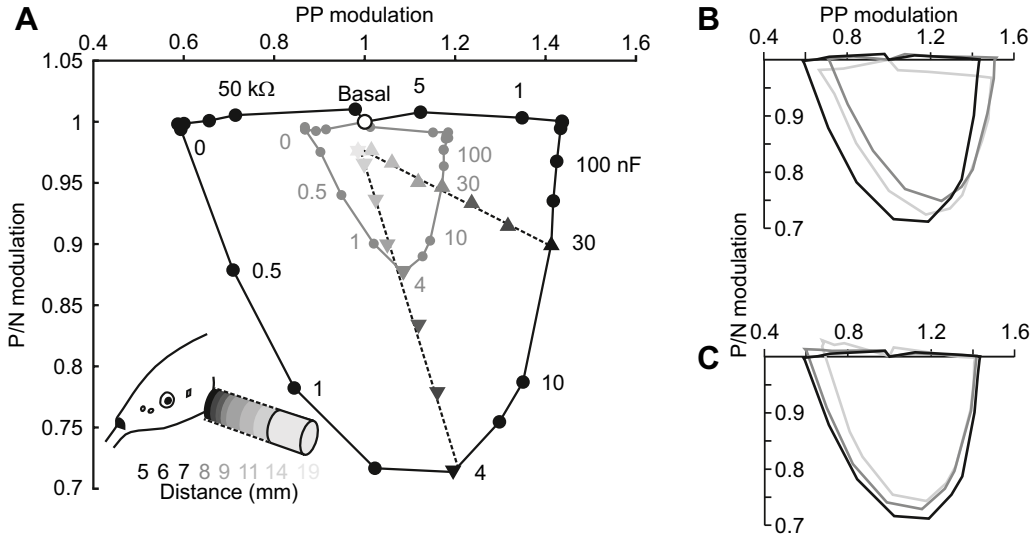


**Fig. 2. Physical stimulus spaces and electric colour lines.** (A) Physical stimulus spaces obtained for a *G. petersii* (recording position is indicated by a grey rectangle to the right of the fish's eye) at 5 mm (black) and 8 mm (grey) object distance. Filled circles indicate mean PP–P/N modulation pairs induced by capacitive and resistive dipole object settings, some of which are indicated. Means were obtained from $n$=20 repetitive lEOD recordings per object setting. The basal PP–P/N condition is indicated by an open circle. Filled triangles show PP–P/N modulation pairs of a 4 and 30 nF dipole object obtained over increasing distance (coded by black to grey shading; see also inset and numbers on the bottom left). The two fitted data sets (dashed lines) show two distinct linear functions (electric colour lines). (B) Stimulus spaces (at 5 mm object distance) of the three experimental animals (shading indicates different fish). (C) Stimulus spaces (at 5 mm distance) of one fish obtained on three different days (shading indicates different recording days).

smaller resistance than that of the water. P/N modulations smaller than 1 indicate a distortion of the local EOD waveform. Note that PP and P/N modulations become stronger the more they deviate from 1 (basal condition). PP–P/N modulation pairs obtained for 5 and 8 mm object distances (Fig. 2A) shaped the borders of two so-called 'physical stimulus spaces' (von der Emde and Ronacher, 1994). The common centre of the two spaces is defined by the basal PP–P/N condition (PP modulation≈1 and P/N modulation≈1). Stimulus spaces decreased with increasing object distance.

PP–P/N modulation pairs of an object (4 or 30 nF, Fig. 2A) recorded at a single skin position and increasing object distances form a distinct linear function. In theory, all the other PP–P/N modulation pairs of the amplitude and waveform images (caused by the same dipole object) would also lie on this specific line. The lines of different objects converge towards the basal PP–P/N condition (with a slight offset; see the two lines in Fig. 2A). The slope of each linear function provides a measure 'electric colour' to obtain the object's impedance, independent of object distance.

As our preliminary results agreed with earlier findings (Budelli and Caputi, 2000; Caputi and Budelli, 2006; von der Emde and Ronacher, 1994; von der Emde and Schwarz, 2002), we chose four capacitive dipole objects (1, 4, 30, 100 nF; see Fig. 2) for electric image measurements.

To ensure that object-evoked modulations obtained for different fish and recording sessions were comparable, we additionally recorded stimulus spaces for the two other experimental animals and for one fish on two additional days. Because results for different fish (Fig. 2B) and different days (Fig. 2C) revealed no considerable variations, it was appropriate to collect electric image data from different animals over a prolonged period of time.

### Natural capacitive objects

As natural capacitive objects, we used: a caddis worm (*Anabolia nervosa*, ∼2 $cm^3$), a zebra fish (*Danio rerio*, ∼2 $cm^3$), an aquatic plant stem (*Anubias* sp., ∼5 $cm^3$) and a tomato (∼14 $cm^3$).

In contrast to the dipole objects, which were made of carbon and an insulating cover, the natural objects had a homogeneous surface. The caddis worm, however, with its protective debris case, soft abdomen and chitinized head, featured a versatile material composition, which is also the case for the dipole objects. Prior to the recordings, the stimulus animals were killed by immersion in a solution of 2 mg $ml^{-1}$ Ethomidate (caddis worm) or 2 g $l^{-1}$ MS 222 (Acros Organics, Geel, Belgium; zebrafish).

### Recording of electric images

For electric image recordings, a spatial measuring grid was used, which forms a vertical plane (18×19 mm) close to the side of the head of the fish (Fig. 3). Objects were aligned in a middle position with respect to the plane's centre (Fig. 3) at various (5, 6.5, 8 mm) object-to-fish distances. The plane centre 9 mm caudal from the fish's eye ($x$ position), at the centre of the eye (dorso-ventral, $y$ position) and 2 mm from the skin (lateral, $z$ position), was used as a positioning reference for the electrode prior to the measurements. During recordings, the electrode was moved in 1 mm ($x$ direction) and 2 mm ($y$ direction) steps, covering the plane with $n$=200 lEOD recording positions (Fig. 3). Acquisition time for a full measurement

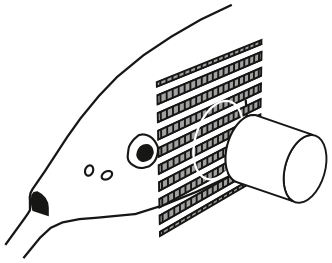

**Fig. 3. Measuring grid to obtain spatial electric images.** lEOD recording positions close to the head of a *G. petersii* ($n$=200) are shown as grey rectangles. The relative alignment of a nearby dipole object (white cylinder) is indicated on the grid as a white circle.

Journal of Experimental Biology (2017) 220, 3142-3153 doi:10.1242/jeb.159244

was several hours (~2.5–3 h). Full spatial resolution of 19×20=380 image pixels was achieved by interpolation of the obtained PP and P/N modulations (from 200 to 380 values). To do so, an interpolated modulation pixel was calculated as the mean modulation of its upper and lower neighbouring pixel on the grid.

### Analysis of electric images

Data analysis and visualization were carried out with custom-written MATLAB (Mathworks, Natick, MA, USA) routines. To characterize the centre-surround (Mexican hat) profile of amplitude and waveform images (Fig. 4A), we analysed the deviation of the object-evoked image modulations from the mean basal PP or P/N condition within the measuring grid, which occurs in the absence of any object. This was obtained by averaging nine basal PP and P/N means, acquired from nine spatial measurements (three for each fish), performed without any object and without data interpolation. The basal PP or P/N condition was then compared with the modulations of object-evoked amplitude or waveform images.

Image modulations that fell in the range of twice the standard deviation of the basal condition (PP=1±0.018, P/N=1±0.005) were determined as basal. Modulations outside this range were considered to be part of the image centre or reverse rim area (Fig. 4B). The image centre was determined as the area that contained the image pixel with the strongest modulation (i.e. with the largest deviation from 1). This parameter is termed the peak amplitude (PA, for amplitude images) or peak distortion (PD, for waveform images). Both parameters are related to the object's impedance but change with the shape, size and distance of the object.

To obtain the relative image slope as a measure for object distance, the absolute maximal or minimal rostral image slope (Fig. 4C) was divided by the peak modulation (PA, PD) of the image centre (Fig. 4A). The relative image slope is termed the slope-to-amplitude ratio (SAR, for amplitude images) or slope-to-distortion ratio (SDR, for waveform images). Note that slopes of an electric image (Fig. 4C) were calculated in the horizontal direction only.

Electric colour of an object was calculated as the slope of a linear function obtained from all PP–P/N modulation pairs ($n$=380) of an amplitude and corresponding waveform image. As illustrated in Fig. 4D, PP–P/N modulation pairs can form a spatial distribution when plotted in a 2D space (with amplitude and waveform on its axis). As such distributions lack a clear linear relationship between amplitude and waveform modulations, a possible electric colour line has to be estimated by further calculations.

Thus, we first identified and labelled PP–P/N modulation pairs that might indicate the path of an electric colour line. To do so, we made two assumptions: (i) the scattering of PP–P/N modulation pairs is related to local form differences of the two electric image profiles (amplitude and waveform); (ii) all PP–P/N pairs obtained from shape-congruent areas of an amplitude and waveform image indicate the path of the electric colour line (Fig. 4D).

To analyse the form of an amplitude or waveform image, it is necessary to normalize their modulation profiles. Normalization was performed by setting the peak modulation (PA or PD) of an electric image to 1, the basal modulation to 0 and by rescaling all other image modulations with respect to these settings.

Local form differences of an amplitude and waveform image were then calculated by subtracting their normalized modulations (PP minus P/N image pixel, pixel by pixel). Only local PP–P/N differences within a range of ±0.1 were considered as shape congruent.

After identifying the shape-congruent and -incongruent areas of an amplitude and waveform image, the PP–P/N modulation pairs obtained by the original (not normalized) electric image profiles were separated according to these two areas. Within the distribution of PP–P/N modulation pairs, plotted in 2D space, the values from shape-congruent image sections were emphasized (Fig. 4D). Electric colour lines were then defined by applying linear fits

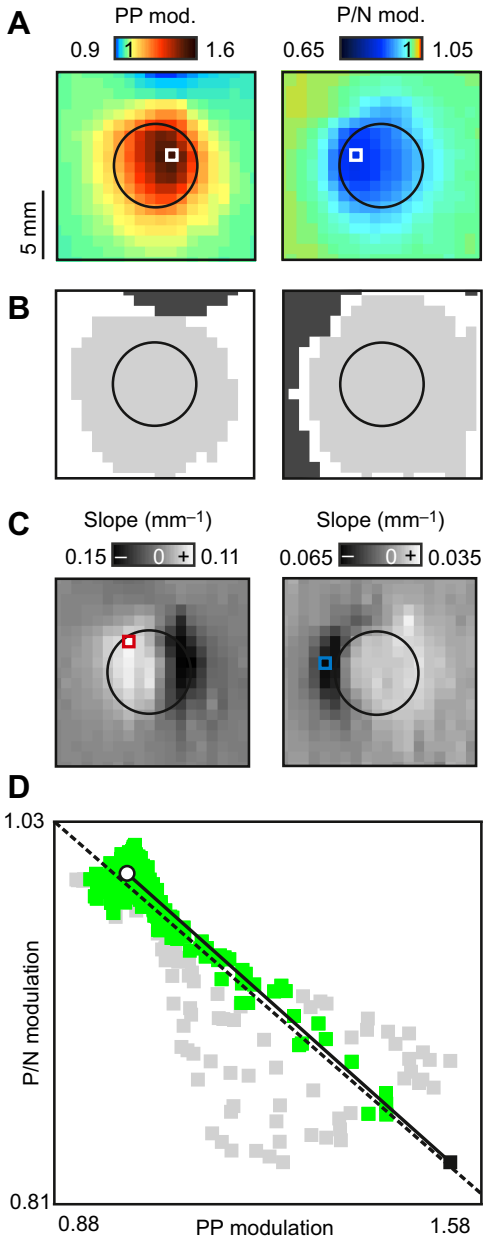


**Fig. 4. Analysis of electric images and image parameters.** (A) Colour-coded amplitude (left) and waveform (right) images of a 30 nF dipole object at 5 mm object distance. Relative object alignment is indicated by a black circle. Peak modulation pixels are marked by rectangles. (B) Mexican hat profiles of the amplitude (left) and waveform (right) image with image centre (grey), rim area (dark grey) and basal areas (white) accentuated. (C) Spatial profiles of the slopes of the amplitude (left) and waveform (right) image. Rostral maximum slope (red rectangle) and rostral minimum slope (blue rectangle) are marked. (D) Distribution of PP–P/N modulation pairs (grey and green rectangles) of combined amplitude and waveform image pixels plotted in 2D space. Green modulation pairs are obtained by a combination of shape-congruent image pixels. The open circle indicates the basal condition; the filled black rectangle indicates the peak modulation pair. Electric colour lines (linear fits) are indicated by a black dashed line (whole data fit) and by a black solid line (fitting the basal and peak modulation pair).

Journal of Experimental Biology (2017) 220, 3142-3153 doi:10.1242/jeb.159244

(i) to the entire distribution of PP–P/N modulation pairs and (ii) only to a peak modulation pair and the basal PP–P/N condition (Fig. 4D). The peak modulation pair was obtained by combining peak amplitude and peak distortion, even though they might originate from different local positions within the electric images (Fig. 4A). Linear functions that matched the labelled electric colour pathway (Fig. 4D) were used to extract electric colour (i.e. slope of the line).

### Data availability

Recorded data and custom-written MATLAB routines used for evaluation are stored on the server of the Zoological Institute/Department of Neuroethology and can be provided by the corresponding author upon request.

## RESULTS

### Spatial profiles of amplitude and waveform images

Electric images obtained for dipole objects (Fig. 5A) and natural capacitive objects (Fig. 5B) had a reverse centre-surround (Mexican hat) profile, as has been reported for amplitude images of purely resistive objects (Caputi et al., 1998).

Interestingly, we found that in addition to amplitude images, waveform images (Fig. 5) also shared this basic electric image organization. However, for most capacitive objects, individual modulation patterns of the two image types (Fig. 5: colour-coded profiles) differed considerably. Hence, variations in size, shape, number and location of the central, basal and rim areas of these Mexican hat profiles (Fig. 5: grey-scale profiles) occurred. Variation among Mexican hat profiles of amplitude images was greater than that of waveform images. Note that for some electric image profiles that greatly exceeded the size of the measuring plane (Fig. 5B), possible outer regions (basal or rim areas) could not be assessed. In almost all amplitude and waveform images (Fig. 5), image centres were obtained near the skin area immediately adjacent to the projecting objects. However, peak modulation pixels (PA, PD) of the central regions of corresponding amplitude and waveform images did not match the same locations. Here, offsets of several (1–9.2) millimetres were observed (except peak modulations obtained for electric images of the caddis worm, which showed no offset; Fig. 5B).

### Distance estimation of capacitive objects

To evaluate whether distance estimation in *G. petersii* is mediated by both amplitude and waveform images, we performed recordings of dipole objects at three different object-to-fish distances (5, 6.5, 8 mm). As different capacitive dipole objects were generated by only changing the internal circuit settings of the dipole cylinder, spatial dimensions and the shape of the objects were constant. Thus, object-evoked electric images were only influenced by the two object parameters impedance and distance. For four capacitive circuit settings of the dipole object, we recorded $n$=5 (4, 30 nF) or $n$=1 (1, 100 nF) electric images for each object distance.

With increasing object distance, the overall modulation profiles of the amplitude and waveform images became weaker but expanded in size (example shown in Fig. 6). Thus, over distance, peak modulations (PA and PD, Fig. 7A1 and B1) were reduced in modulation strength (deviation from 1) and rostral image slopes became less steep (Fig. 7A2 and B2). Both image parameters were also influenced by object impedance (Fig. 7).

When image slopes were divided by the peak modulations (PA or PD), variations due to object impedance were almost cancelled out for relative slopes of amplitude images (SAR; see Fig. 7A3). In contrast, SDRs (Fig. 7B3) of waveform images were still altered by distance and the capacitive settings of the dipole object. Thus, only the relative slopes of amplitude images provided unequivocal distance cues independent of object impedance.

### Impedance estimation of capacitive objects

Two strategies of processing electric image parameters were suggested that might enable *G. petersii* to measure object impedance irrespective of object distance.

A first strategy we address is based on the calculation of the peak modulations (PA, PD) of amplitude and waveform images and an additional calibration routine. Here, we combined the SAR of amplitude images with the peak modulations of amplitude (PA) and waveform images (PD). SDRs were not used for the calibration routine, as they were not unequivocal distance measures.

For each capacitive dipole object setting (1, 4, 30, 100 nF) and object distance (5, 6.5, 8 mm), PA and PD were first plotted versus the SAR (Fig. 8). Over distance, the relationship of peak modulation (PA, PD) and SAR was linear, revealing distinct functions for each capacitive dipole object. Note that linear functions with a close or overlapping alignment (e.g. the two lines of the 30 and 100 nF object in Fig. 8A) occurred for capacitive dipole objects that generated similar peak modulations (compare PA of the 30 and 100 nF object in Fig. 7A1).

The slopes of the lines provide distance-invariant measures for object resistance (PA data set, Fig. 8A) or capacitance (PD data set, Fig. 8A). Both slope values enable distance-invariant impedance estimation when combined.

To obtain such slope values, the fish has to relate the SAR and peak modulations (PA, PD), gained by a successive sequence of electric images, when approaching the object. The distance passed between the acquisition of two successive amplitude and waveform images needed to calculate a slope value may vary as a result of the actual swimming speed and EOD rhythm of the animal. Fig. 8B shows slope values calculated for different distance intervals resulting from varying combinations of two SAR–PA or SAR–PD pairs that were obtained for the three object distances mentioned above. The slope values depended on the capacitive settings of the dipole objects and showed no considerable variation for different distance intervals. The modulation direction (larger or smaller than 1) and the relative modulation strength (deviation from 1) of the original peak modulations (Fig. 7A1,B1) were preserved by the slope values (Fig. 8B). They are now encoded by the direction (positive or negative) and the steepness of the slope.

As an alternative to the dynamic calibration mechanism outlined above, which requires movement of the fish or the object, we propose a second strategy, which uses a static parameter for obtaining the impedance of an object: electric colour. It can be extracted from a single pair of amplitude and waveform images, obtained from a stationary position. Fig. 9 shows the PP–P/N modulation pair distributions obtained from artificial and natural objects with a distance of 5 mm from the fish's head.

Most distributions showed varying amounts of scatter, indicating that, for most of the objects tested, PP–P/N pairs did not form a defined electric colour line. However, the PP–P/N pairs of shape-congruent areas of amplitude and waveform images, labelled within a distribution, clearly indicate a linear pathway, which we propose corresponds to the path of an electric colour line. In addition, a clear linear function (colour line) formed when almost exclusively shape-congruent PP–P/N pairs were obtained (by electric images of a zebrafish, see Fig. 9B).

To extract electric colour lines from a PP–P/N pair distribution, we applied linear fits to either the whole distribution or only the



Journal of Experimental Biology

Journal of Experimental Biology (2017) 220, 3142-3153 doi:10.1242/jeb.159244

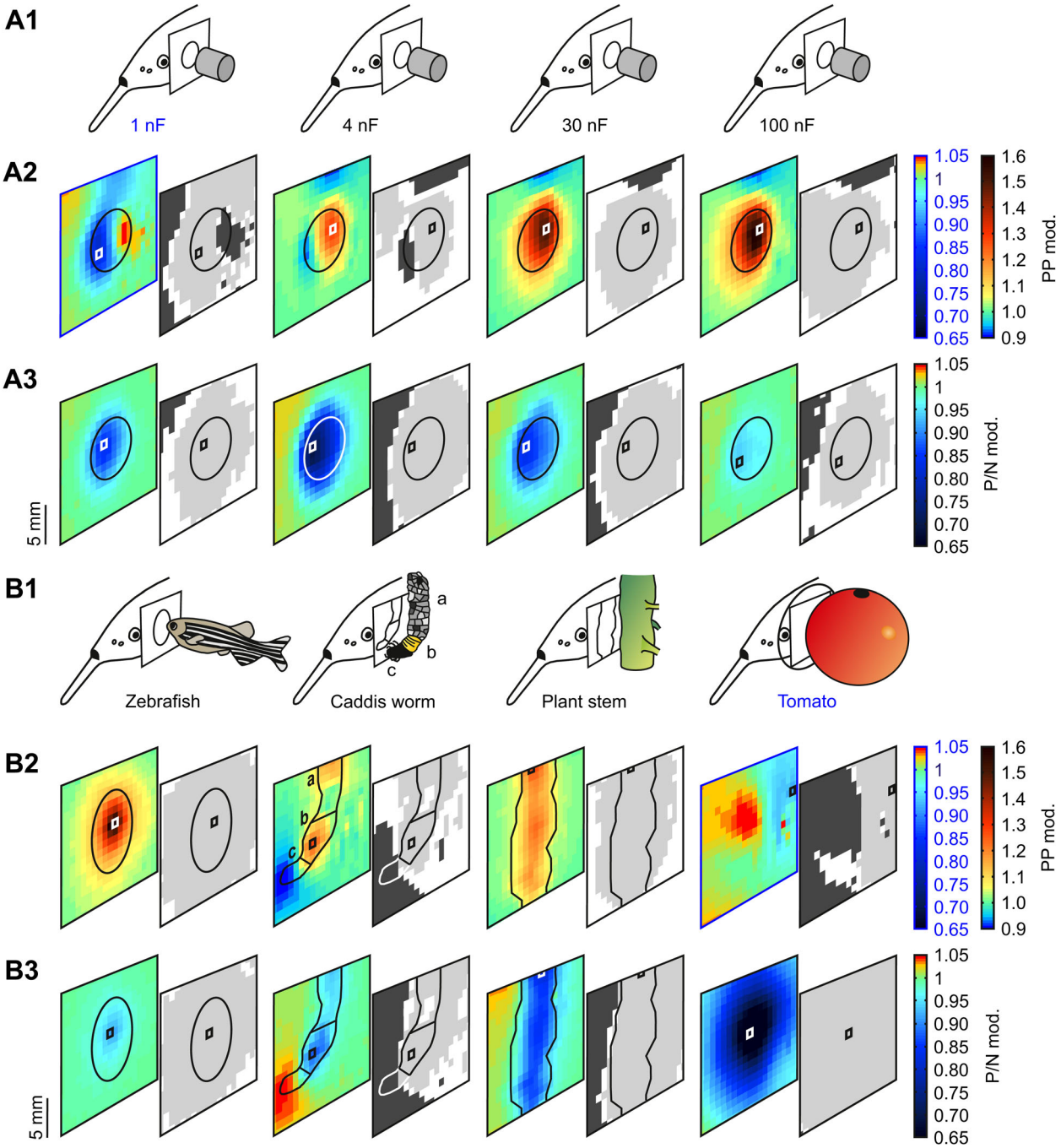


**Fig. 5. Electric images of dipole and natural objects at 5 mm object distance.** (A) Dipole objects. (A1) Schematic drawing indicating the alignment (black circles) of the dipole objects (grey cylinders) relative to the measuring plane. Circuit settings are given below. (A2) Amplitude images are shown colour coded (left) and with accentuated areas – centre (light grey), basal areas (white) and rim areas (dark grey) – of the Mexican hat profile (right). The colour scale indicated in blue belongs to the 1 nF object (labelled in blue). Peak amplitude pixels (rectangles) and relative object alignments (circles) are indicated. (A3) Waveform images shown in the same manner as described in A2, with analogue markings (rectangles indicate peak distortion pixels). (B) Natural objects. (B1) Schematic drawing indicating the alignment of natural objects relative to the measuring plane (see black markings on plane). For the caddis worm, the alignment of its different body sections – (a) debris case, (b) abdomen, (c) head – is indicated as three different areas on the plane. (B2) Amplitude images of natural objects shown in the same manner as in A2. The colour scale indicated in blue belongs to the tomato (labelled in blue). (B3) Waveform images of natural objects arranged as in A3 with analogue markings.

peak modulation pair of the distribution and the basal PP–P/N condition. Judging the performance of both methods by matching the obtained lines with the electric colour pathway, we found that linear functions due to fitting the basal and peak modulation pair had an accurate alignment for all distributions (of natural and dipole objects), whereas lines of whole data fits did not (see, for example, the tomato in Fig. 9B). For further evaluations, we therefore limited extraction of electric colour (i.e. the slope of the line) to linear functions gained by fitting the peak modulation pair and basal condition.

To explore distance invariance of electric colour, we analysed the electric images of capacitive dipole objects that were previously



Journal of Experimental Biology

Journal of Experimental Biology (2017) 220, 3142-3153 doi:10.1242/jeb.159244

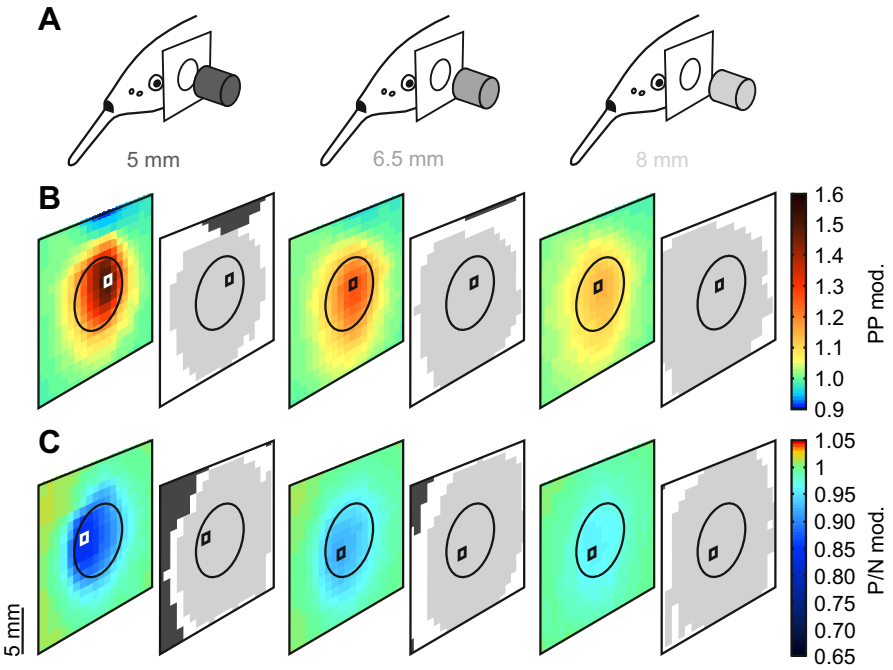


**Fig. 6. Electric images of a 30 nF dipole object at 5, 6.5 and 8 mm object distance.** (A) Schematic drawing of distance (indicated by dark to light grey object shading and numbers) and relative object alignment to the measuring plane (black circles on plane). (B) Amplitude images shown colour coded (left) and with white-to-grey shading indicating areas of the Mexican hat profile as described in Fig. 5. Rectangles indicate peak amplitude pixels. Relative object alignment is shown as in A. (C) Waveform images arranged as in B with analogue markings (rectangles show peak distortion pixels).

used to determine the calibration mechanism for impedance estimation based on relative image slopes (see Fig. 8).

We found a set of distinct electric colour lines for the different capacitive dipole objects tested (Fig. 10A). The different electric colour lines obtained for a given dipole object showed only slight variation in their relative alignment. These variations, as observable in the data with multiple measurements of a dipole object (4 and 30 nF objects), systematically decreased with further distance.

Electric colours extracted from the linear functions as slope values (Fig. 10B) did not change considerably for different object distances, but were scaled by the capacitive settings of the dipole object.

Thus, in accordance with simulation data from Budelli and Caputi (2000), we found electric colour to be a distance-invariant impedance estimator. In addition, we could show that extraction of electric colour by relating just a peak modulation pair to the basal condition was more accurate than incorporating all modulation pairs of amplitude and waveform images.

## DISCUSSION

In the present paper, we addressed the unambiguous analysis of capacitive objects during active electrolocation in *G. petersii*. We specifically focused on electric imaging principles enabling estimation of object distance and impedance independent of one another. To our knowledge, this is the first study on active electrolocation in mormyrid fish providing extensive measurements of high-resolution amplitude and waveform images of artificial and natural capacitive objects.

We show that both electric image types have a Mexican hat profile. Electric image analysis indicated that the relative slope of amplitude images (SAR) is the only impedance-invariant distance estimator. Combining the peak modulation of both image types with the SAR, we established a dynamic calibration mechanism providing stable impedance measures over distance. Distance-independent impedance estimation was also possible by using electric colour as a static measure. We found that a reliable estimation of electric colour can be obtained by combining the peak modulation of both image types and the basal amplitude and waveform condition, obtained in the absence of an object.

### Spatial profiles of amplitude and waveform images

Our approach of processing amplitude and waveform modulations as topographically ordered electric images is strongly supported by the structural and functional organization of the electrosensory pathway in the brain of *G. petersii*.

In these fish, the receptor-encoded EOD amplitudes and waveforms from the fish skin are transmitted via afferent fibres to the neuronal network of the electrosensory lateral line lobe (ELL), a cerebellum-like structure in the hindbrain (Bell, 1990; Meek et al., 1999). Amplitude information (A-cell afferents) is projected to the medial zone of the ELL, whereas amplitude and waveform information combined (B-cell afferents) is relayed to the dorso-lateral zone. Both zones constitute somatotopic maps of the electroreceptive body surface (Maler et al., 1973). The object-evoked excitation pattern within both ELL zones is processed jointly with an efference copy of the EOD, termed electric organ corollary discharge (EOCD) (Bell, 1989). The EOCD is modifiable by previous sensory experience, such as stimuli in the absence of an object (Bell, 1989; Bell et al., 1997). The circuitry is thus sufficient to provide the modulations caused by the object-evoked peripheral stimulus profile from the fish skin. Following this concept, topographical amplitude images are directly gained from the modulation patterns within the ELL medial zone. Determination of waveform images, however, requires a combined processing (subtraction) of the modulation patterns of both ELL zones at a higher level (von der Emde and Bell, 1994). Anatomical studies indeed have shown that projections from the two ELL zones converge at the nucleus lateralis in the fish's midbrain (Bell, 1981; Hollmann et al., 2016). Moreover, these studies provided evidence of a somatotopic midbrain map, from which topographical waveform images could be acquired. The somatotopic organization at the level of the midbrain, however, was found to be much weaker than in the ELL network (Hollmann et al., 2016).

During our recordings, image acquisition was mainly performed close to the electro-receptive areas of the fish's head. The obtained image profiles thus appropriately represent the sensory information that is actually perceived by the animal. However, it should be mentioned that the influence of skin curvature on the peripheral



Journal of Experimental Biology

Journal of Experimental Biology (2017) 220, 3142-3153 doi:10.1242/jeb.159244

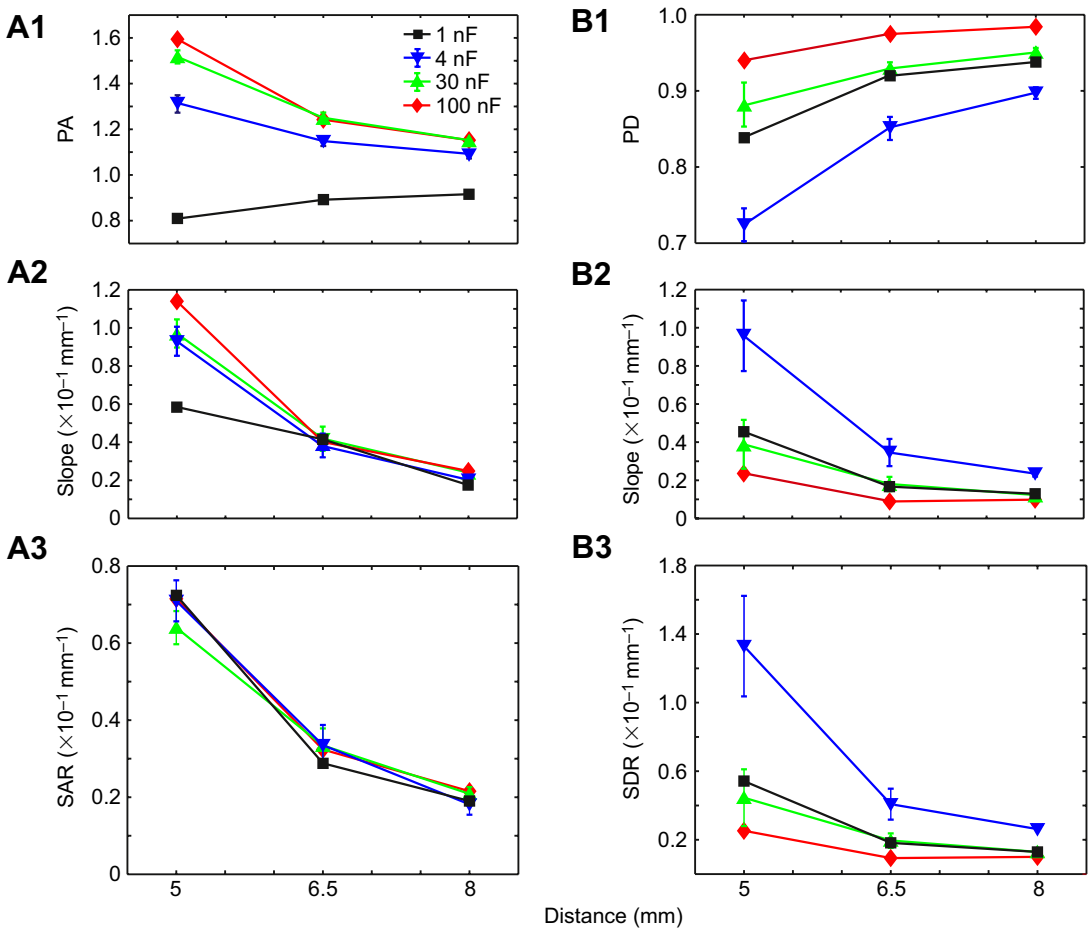


**Fig. 7. Relationship of amplitude and waveform image parameters to object impedance and distance.** Coloured symbols show means±s.d. of parameters obtained during *n*=5 single image recordings (for 4 and 30 nF dipole objects), or single values (*n*=1, obtained for 1 and 100 nF objects). (A) Amplitude image parameters. (A1) Peak amplitudes (PA) of amplitude images. (A2) Maximal rostral image slopes of amplitude images (absolute values). (A3) Relative slopes of amplitude images (SAR, slope-to-amplitude ratio). (B) Waveform image parameters. (B1) Peak distortions (PD) of waveform images. (B2) Minimal rostral slopes of waveform images (absolute values). (B3) Relative slopes of waveform images (SDR, slope-to-distortion ratio).

image profiles (Hofmann et al., 2012) could not be accounted for in detail in this study because of the planar recording grid used.

As we have shown in this study, not only amplitude but also waveform images constitute Mexican hat profiles (Fig. 5). They were generated by capacitive objects (natural and artificial) with an outer surface of homogeneous or diverse material composition. Even though the centre-surround (Mexican hat) organization of electric images appears to be a general feature, the effects that yield these profiles are multiple. A capacitive object (water plant, Fig. 5B) with a conducting, homogeneous surface focuses the electric field lines on the fish's skin and a central area of increased lEOD amplitudes and a reverse rim area of decreased lEOD amplitudes is generated. Thus, an amplitude image with central modulations larger than 1 and rim modulations smaller than 1 is produced. In contrast, an object with a homogeneous high-impedance cover (tomato, Fig. 5B) that spreads the field lines on the fish's skin, generates an opposite image profile.

If a capacitive object features a combination of high and low conducting materials (e.g. dipole objects or the caddis worm, Fig. 5), their local opposing effects on the electric field (concentration versus scatter) add up to shape the Mexican hat profile. Thus, in some cases (4 and 1 nF dipole objects) more-complex amplitude image profiles can form with one central but several divided rim areas. For the 1 nF setting, electric field attraction by the dipole object's two carbon poles is low. Field lines are mainly scattered towards the fish's skin by the insulating surface of the object. An amplitude image with central modulations below 1 and reverse rim areas is induced. In the 4 nF dipole object, attraction of the electric field by the poles is stronger so that field lines are concentrated on the fish's skin rather than scattered by the insulating cover. Thus, the amplitude image features central modulations larger than 1 and rim modulations smaller than 1. Our results therefore show that many different configurations of amplitude images exist for capacitive objects.

In contrast, Mexican hat profiles of waveform images (Fig. 5) only show one basic configuration. When capacitive objects interact with the electric field, a capacitance is charged by the positive lEOD phase and discharged by the negative lEOD phase (Budelli et al., 2002). Thus, at a central area on the fish's skin, local EODs are reduced in their initial phase and enlarged in their second phase. Such waveform distortions only cause local reductions of the P/N ratio and modulations of smaller than 1 in the centre of waveform images. Waveform modulations at the reverse rim areas therefore are always larger than 1.

### Distance estimation of capacitive objects

When object distance increases, Mexican hat profiles of amplitude and waveform images undergo multiple changes. As indicated

Journal of Experimental Biology (2017) 220, 3142-3153 doi:10.1242/jeb.159244

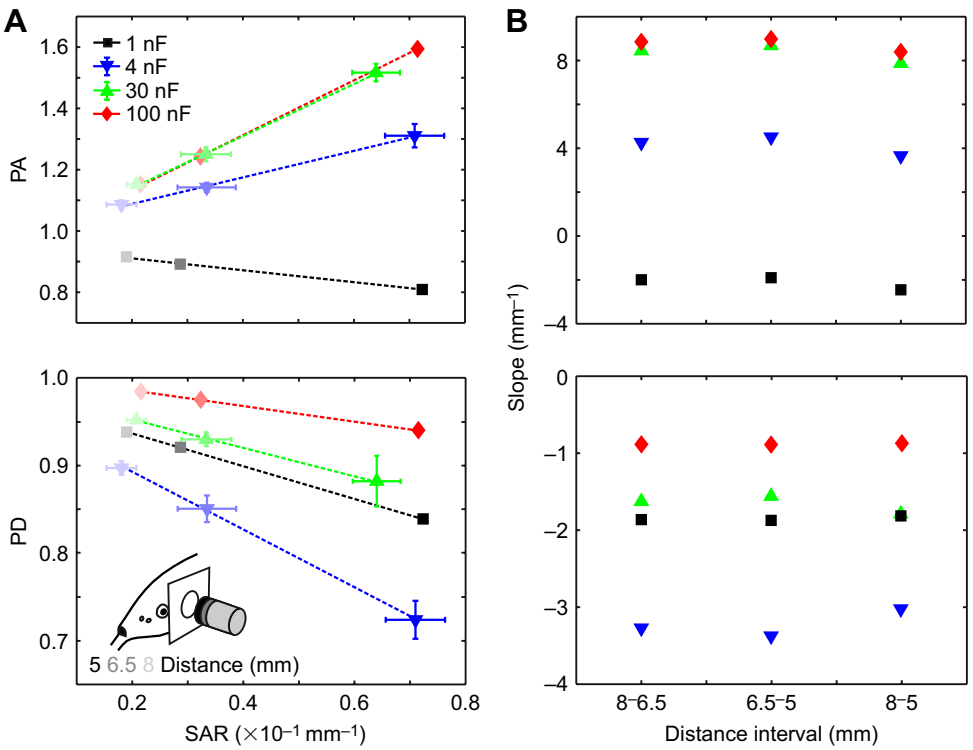


**Fig. 8. Impedance measures dynamically obtained over distance from the relationship of peak modulation and SAR.** (A) PA (top) and PD (bottom) as linear functions of SAR. Coloured symbols indicate capacitive dipole object settings and show means±s.d. of image parameters obtained from *n*=5 image recordings, or single values (*n*=1). Colour intensity of the symbols codes for three object distances (as shown in the inset on the bottom left for the 1 nF object). Linear data fits are indicated as dashed lines. (B) Slopes extracted from the data sets in A for different distance intervals (amplitude data, top; waveform data, bottom).

by the local image features peak modulation and rostral image slope in Fig. 7, modulation strength and image steepness are reduced, while the overall profile spreads out, as shown in Fig. 6. Both image features are also influenced by the impedance of capacitive objects (Fig. 7).

As *G. petersii* relies on the ambiguous electric image input for short-range distance estimation, it needs to consider these multi-parametric effects to obtain a definite distance estimator. Behavioural, simulation and image recording studies (Hofmann et al., 2012; Sicardi et al., 2000; von der Emde et al., 1998) all

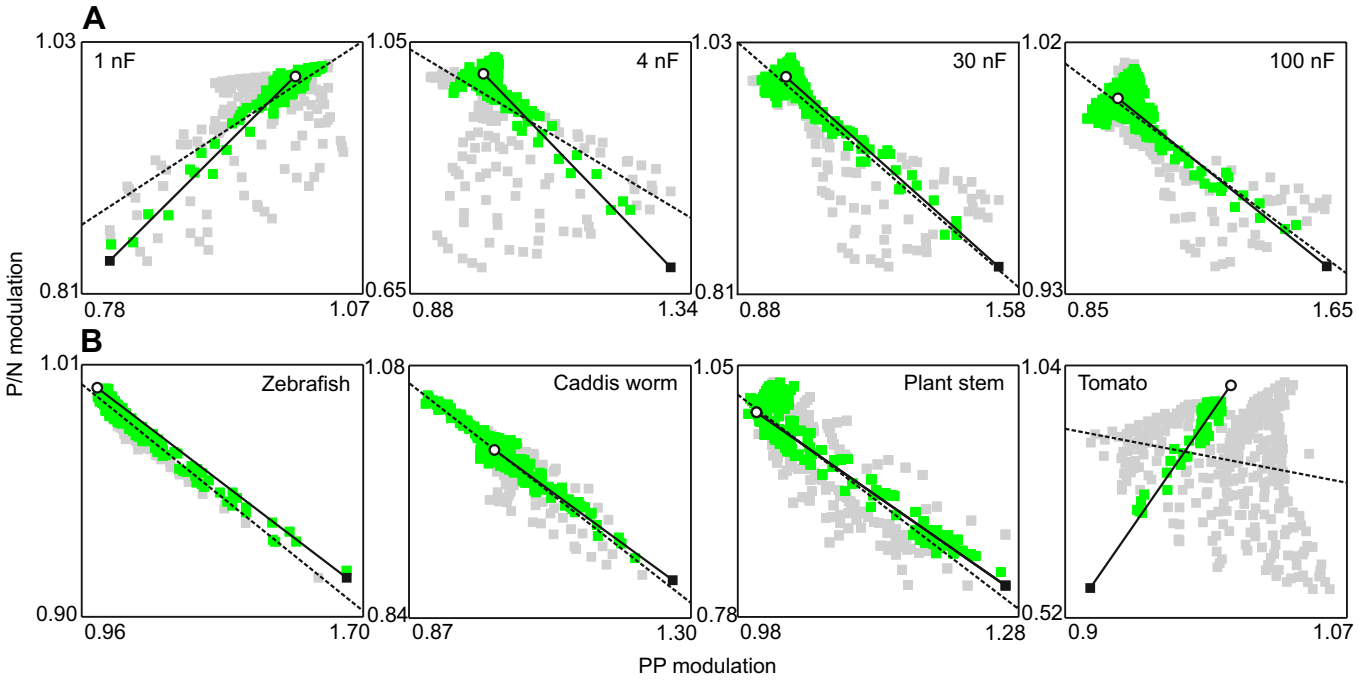


**Fig. 9. Electric colour lines gained by the PP–P/N relationship of amplitude and waveform images of capacitive objects at 5 mm object-to-fish distance.** (A) Distribution of PP–P/N modulation pairs (grey and green rectangles) of electric images of dipole objects (circuit settings are given in the top corners). Green rectangles are PP–P/N modulation pairs of shape-congruent amplitude and waveform image pixels, labelling electric colour pathways of a distribution. Open circles indicate basal conditions, and black rectangles show peak modulation pairs. Linear fits (electric colour lines) are indicated by black dashed lines (whole data fits) and by black solid lines (fitting basal and peak modulation pairs). (B) Distribution of PP–P/N modulation pairs of electric images of natural capacitive objects shown in the same manner as in A.



Journal of Experimental Biology

Journal of Experimental Biology (2017) 220, 3142-3153 doi:10.1242/jeb.159244

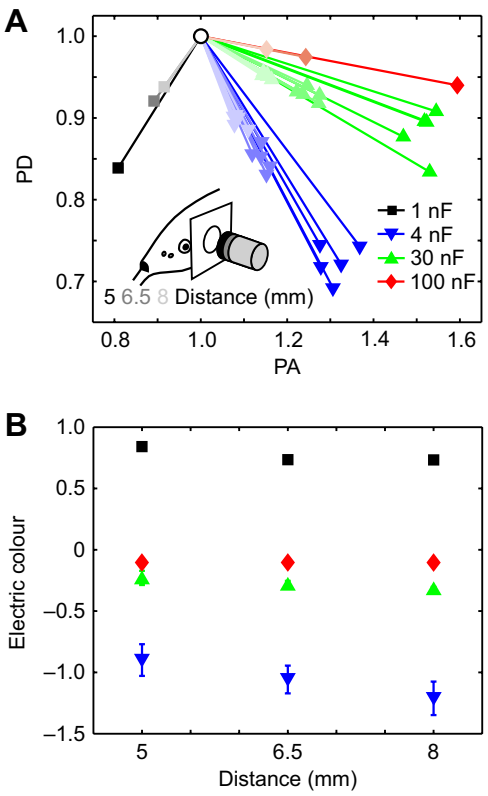


**Fig. 10. Electric colour lines and colour values extracted from the relationship of peak modulation pairs of amplitude and waveform images and the basal condition.** (A) Electric colour lines gained from $n$=5 or $n$=1 image recordings for different capacitive dipole objects (indicated by coloured symbols). Colour intensity of the symbols codes for three object distances, as shown in the inset on the bottom left for the 1 nF object. The basal condition is indicated as an open circle. (B) Electric colour values extracted as the slopes of the linear functions shown in A. Means±s.d. from $n$=5 values or single ($n$=1) values are shown.

suggest that the animals use the relative slope of amplitude images (SAR) to judge the distance of resistive objects. The SAR was shown to be independent of object size and resistance, whereas certain strong variations in object shape affected the SAR in addition to object distance (Sicardi et al., 2000; von der Emde et al., 1998). Because capacitive objects (Fig. 5) like purely resistive objects induce amplitude images, the SAR might be the general distance estimator during active electrolocation in *G. petersii*. Our results obtained for capacitive dipole objects (Fig. 7A3) support this concept. Having excluded effects due to object size and shape in the experiments, we found the SAR to change with distance but not with object capacitance.

As capacitive objects also induce waveform images, we hypothesized an analogue mechanism for estimating object distance by SDRs. Hence, when the SAR might be difficult to extract, e.g. in case of capacitive objects causing only very weak, noisy amplitude images, such a backup cue could improve distance estimation. Our results, however, showed that the SDR was affected by the distance and capacitance of dipole objects (Fig. 7B3). Thus, waveform images are unlikely to provide reliable distance estimations, which in turn appear to be exclusively possible by using relative slopes of amplitude images.

The small receptive fields (Metzen et al., 2008) of ELL neurons, which process amplitude images, are well suited for encoding local image features such as the peak amplitude or a single, dominant edge contrast (i.e. the steepest rostral image slope). Topographically specific mechanisms of lateral inhibition provided by ELL interneurons (Meek et al., 1999, 2001) might further improve this task by enhancing electric image contrast (von der Emde and Engelmann, 2011). In comparison, the weak somatotopic organization of the midbrain map in the lateral nucleus (Hollmann et al., 2016), which may provide only coarse waveform images, might not enable a reliable and precise edge detection circuit. Based on our electric image analysis and the anatomical and physiological findings just mentioned, we conclude that distance perception in *G. petersii* is based on amplitude image information and is mediated only at an early processing stage of the electrosensory pathway.

### Impedance estimation of capacitive objects

Impedance information is crucial for *G. petersii* to identify capacitive prey items (insect larva) buried in the electrically resistive ground (sand, stones) or to discriminate among capacitive objects (for example, other animals, plants, etc.). Object impedance is encoded by the two physical stimulus dimensions lEOD amplitude and waveform, which can be perceived by the animal (von der Emde, 1990; von der Emde and Bleckmann, 1992). A behavioural study by von der Emde and Ronacher (1994) showed that the two stimulus dimensions are perceived independently and weighted equally during discrimination of capacitive objects.

The peak modulations of amplitude (PA) and waveform (PD) images might be the most prominent features for impedance estimation as they represent the strongest change of both stimulus dimensions evoked by an object. However, to turn them into unambiguous impedance estimators, fish need to compensate for additional influences of object size, shape and distance.

In this paper, we introduced a possible mechanism to calibrate peak modulations against object distance. This mechanism implies that the fish integrates the SAR with the PA and PD to accomplish this task. Our data show that when this ‘integration’ of SAR and peak modulations is performed dynamically over certain distance intervals, linear functions are generated whose slopes constitute calibrated impedance measures. The slopes, or ‘calibrated’ PA and PD, are distance invariant while maintaining the relative strength and direction of the original peak modulations (Fig. 8). To obtain such dynamic, motion-related cues by consecutive electric images, fish might simply approach an object or employ distinct scanning behaviours nearby. Observations during behavioural tests indeed indicated that *G. petersii* performs stereotyped movements, so-called probing motor acts (Toerring and Moller, 1984), when judging the impedance of capacitive dipole objects (von der Emde and Ronacher, 1994). The use of motion-related parameters by *G. petersii* has also been emphasized recently in various studies on electrosensory flow (Hofmann et al., 2012, 2016).

Even though such egomotions could suggest a dynamic approach for impedance estimation, a stationary assessment of object impedance due to electric colour (Budelli and Caputi, 2000) also agrees with the behavioural data reported by von der Emde and Ronacher (1994). According to simulation data by Budelli and Caputi (2000), electric colour defines the ‘proportionality’ of amplitude and waveform image modulations (measured as the slope of their linear relationship). It is independent of object distance and scaled by object capacitance. This was also the case for our recorded electric colour data (Fig. 10), which showed no considerable changes over distance, but were altered by object impedance.

However, we found that local shape differences between amplitude and waveform images heavily influence electric colour extraction (Fig. 9). As the two image types allow for different levels of variety in appearance and composition of their Mexican hat profiles (Fig. 5), such shape differences may occur frequently and for several kinds of capacitive objects (with homogeneous or diverse outer covers). With these objects, electric colour is distorted by noise as the paired amplitude and waveform image modulations spread out as spatial distributions instead of forming a straight electric colour line (Fig. 9). Even though we could show that modulations of the shape-congruent image areas sufficiently depict the linear amplitude–waveform relationship (electric colour), we do not expect the fish to be able to determine such modulations, as this would require some complex image normalization procedures (see Materials and methods). Instead, we propose a much simpler mechanism, which provides a robust extraction of electric colour, even for extreme noisy amplitude–waveform distributions (Fig. 9B, tomato). In our algorithm, the image peaks (PA and PD) define the slope of the line (electric colour) in relation to its origin, the basal PP–P/N condition (Fig. 9).

Besides our findings, the anatomical and physiological organization of the electrosensory pathway in the fish's brain may give a first hint whether such an algorithm might be applicable. When compared, the topographic organization of the amplitude map (ELL medial zone) appears much more distinct than that of the proposed waveform map (nucleus lateralis) (Hollmann et al., 2016). Because of this difference, it appears unlikely that a precise topographical and 'hardwired' combination of amplitude and waveform modulations takes place to obtain electric colour information.

In contrast, the calculation of peak modulation by, for example, the mean activity of a population of neurons (von der Emde and Engelmann, 2011) should be unaffected by different levels of somatotopy within each map. It should also compensate for the local offsets observed for PA and PD (Fig. 5A,B). When this output is related jointly to the basal amplitude and waveform condition at a higher level, electric colour could indeed be processed as a slope value by simple consecutive neuronal circuits. Moreover, it might be sufficient to extract electric colour just as a single ratio of the two peak modulations (PA and PD).

In summary, our image data and processing results show that two different mechanisms are applicable for *G. petersii* to measure object impedance irrespective of distance. While they are achieved by different strategies (dynamic versus static imaging), they appear to be based upon the same basic image features PA and PD. The two approaches may also add different qualities to impedance estimation.

While its behavioural relevance is not explicitly proven, electric colour provides the relationship of both signal dimensions (amplitude and waveform). For a comparison of capacitive objects, however, it has already been shown that the animal can additively combine these two signal dimensions (von der Emde and Ronacher, 1994). Fish therefore analyse the combined stimulus intensity induced by an object, which can be called 'electric brightness' by analogy to vision. To judge electric brightness irrespective of object distance, fish could sum the 'calibrated' peak amplitude (PA) and peak distortion (PD) by an algorithm implemented in the midbrain. Alternatively, electric brightness may already be available from the dorso-lateral ELL map, which receives joint amplitude and waveform information from B-cell afferents. In this case, we suggest that the dynamic SAR-based calibration procedure applied to the peak of such a modulation map would provide a similar, distance-independent brightness parameter.

**Acknowledgements**
We thank Sven Rau for his help on developing the custom LabVIEW program used for electric image recordings.

**Competing interests**
The authors declare no competing or financial interests.

**Author contributions**
Conceptualization: M.G., G.v.d.E.; Methodology: M.G., G.v.d.E.; Software: M.G.; Formal analysis: M.G.; Investigation: M.G., R.A.B.; Resources: G.v.d.E.; Writing - original draft: M.G.; Writing - review & editing: M.G., G.v.d.E.; Visualization: M.G.; Supervision: G.v.d.E.; Project administration: G.v.d.E.; Funding acquisition: G.v.d.E.

**Funding**
This work was supported by the Graduate School BIONICS of the Deutsche Forschungsgemeinschaft [GRK 1572 to M.G., R.A.B. and G.v.d.E.].

**References**

**Bell, C. C.** (1981). Central distribution of octavolateral afferents and efferents in a teleost (Mormyridae). *J. Comp. Neurol.* **195**, 391-414.
**Bell, C. C.** (1989). Sensory coding and corollary discharge effects in mormyrid electric fish. *J. Exp. Biol.* **146**, 229-253.
**Bell, C. C.** (1990). Mormyromast electroreceptor organs and their afferent fibers in mormyrid fish. II. Intra-axonal recordings show initial stages of central processing. *J. Neurophysiol.* **63**, 303-318.
**Bell, C., Bradbury, J. and Russell, C.** (1976). The electric organ of a mormyrid as a current and voltage source. *J. Comp. Physiol. A* **110**, 65-88.
**Bell, C. C., Caputi, A. and Grant, K.** (1997). Physiology and plasticity of morphologically identified cells in the mormyrid electrosensory lobe. *J. Neurosci.* **17**, 6409-6423.
**Budelli, R. and Caputi, A. A.** (2000). The electric image in weakly electric fish: perception of objects of complex impedance. *J. Exp. Biol.* **203**, 481-492.
**Budelli, R., Caputi, A., Gomez, L., Rother, D. and Grant, K.** (2002). The electric image in *Gnathonemus petersii*. *J. Physiol. Paris* **96**, 421-429.
**Caputi, A. A. and Budelli, R.** (2006). Peripheral electrosensory imaging by weakly electric fish. *J. Comp. Physiol. A* **192**, 587-600.
**Caputi, A. A., Budelli, R., Grant, K. and Bell, C. C.** (1998). The electric image in weakly electric fish: physical images of resistive objects in *Gnathonemus petersii*. *J. Exp. Biol.* **201**, 2115-2128.
**Engelmann, J., Bacelo, J., van den Burg, E. and Grant, K.** (2006). Sensory and motor effects of etomidate anesthesia. *J. Neurophysiol.* **95**, 1231-1243.
**Harder, W.** (1968). Die beziehungen zwischen elektrorezeptoren, elektrischem organ, seitenlinienorganen und nervensystem bei den Mormyridae (Teleostei, Pisces). *Z. Vergl. Physiol.* **59**, 272-318.
**Harder, W., Schief, A. and Uhlemann, H.** (1964). Zur Funktion des elektrischen Organs von Gnathonemus petersii (Gthr. 1862) (Mormyriformes, Teleostei). *Z. Vergl. Physiol.* **48**, 302-331.
**Hofmann, V., Sanguinetti-Scheck, J. I., Gómez-Sena, L. and Engelmann, J.** (2012). From static electric images to electric flow: towards dynamic perceptual cues in active electroreception. *J. Physiol. Paris* **107**, 1-12.
**Hofmann, V., Sanguinetti-Scheck, J. I., Gomez-Sena, L. and Engelmann, J.** (2016). Sensory flow as a basis for a novel distance cue in freely behaving electric fish **37**, 302-312.
**Hollmann, V., Hofmann, V. and Engelmann, J.** (2016). Somatotopic map of the active electrosensory sense in the midbrain of the mormyrid *Gnathonemus petersii*. *J. Comp. Neurol.* **524**, 2479-2491.
**Maler, L., Karten, H. J. and Bennett, M. V. L.** (1973). The central connections of the posterior lateral line nerve of *Gnathonemus petersii*. *J. Comp. Neurol.* **151**, 57-66.
**Meek, J., Grant, K. and Bell, C.** (1999). Structural organization of the mormyrid electrosensory lateral line lobe. *J. Exp. Biol.* **202**, 1291-1300.
**Meek, J., Hafmans, T. G. M., Han, V., Bell, C. C. and Grant, K.** (2001). Myelinated dendrites in the mormyrid electrosensory lobe. *J. Comp. Neurol.* **431**, 255-275.
**Metzen, M. G., Engelmann, J., Bacelo, J., Grant, K. and von der Emde, G.** (2008). Receptive field properties of neurons in the electrosensory lateral line lobe of the weakly electric fish, *Gnathonemus petersii*. *J. Comp. Physiol. A* **194**, 1063-1075.
**Sicardi, E. A., Caputi, Á. A. and Budelli, R.** (2000). Physical basis of distance discrimination in weakly electric fish. *Physica A* **283**, 86-93.
**Szabo, T. and Wersäll, J.** (1970). Ultrastructure of an electroreceptor (mormyromast) in a mormyrid fish, *Gnathonemus petersii*. II. *J. Ultrastruct. Res.* **30**, 473-490.
**Toerring, M.-J. and Moller, P.** (1984). Locomotor and electric displays associated with electrolocation during exploratory behavior in mormyrid fish. *Behav. Brain Res.* **12**, 291-306.
**von der Emde, G.** (1990). Discrimination of objects through electrolocation in the weakly electric fish, *Gnathonemus petersii*. *J. Comp. Physiol. A* **167**, 413-421.
**von der Emde, G. and Bell, C. C.** (1994). Responses of cells in the mormyrid electrosensory lobe to EODs with distorted waveforms: implications for capacitance detection. *J. Comp. Physiol. A* **175**, 83-93.

**von der Emde, G. and Bleckmann, H.** (1992). Differential responses of two types of electroreceptive afferents to signal distortions may permit capacitance measurement in a weakly electric fish, *Gnathonemus petersii*. *J. Comp. Physiol. A* **171**, 683-694.

**von der Emde, G. and Engelmann, J.** (2011). Active electrolocation. In *Encyclopedia of Fish Physiology: From Genome to Enviroment* (ed. A. P. Farrell), pp. 375-386. San Diego: Elsevier Inc.

**von der Emde, G. and Ronacher, B.** (1994). Perception of electric properties of objects in electrolocating weakly electric fish: two-dimensional similarity scaling reveals a City-Block metric. *J. Comp. Physiol. A* **175**, 801-812.

**von der Emde, G. and Schwarz, S.** (2002). Imaging of Objects through active electrolocation in *Gnathonemus petersii*. *J. Physiol. Paris* **96**, 431-444.

**von der Emde, G., Schwarz, S., Gomez, L., Budelli, R. and Grant, K.** (1998). Electric fish measure distance in the dark. *Nature* **395**, 890-894.